

GRAVITATIONAL LENSING BY BLACK HOLES: A COMPREHENSIVE TREATMENT AND THE CASE OF THE STAR S2

V. BOZZA^{1,2,3} AND L. MANCINI^{2,3,4}

Received 2004 March 3; accepted 2004 April 27

ABSTRACT

Light rays passing very close to a black hole may experience very strong deviations. Two geometries have been separately considered in recent literature: a source behind the black hole (standard gravitational lensing) and a source in front of the black hole (retrolensing). In this paper we start from the strong-field limit approach to recover both situations under the same formalism, describing not only the two geometries just mentioned but also any possible intermediate configurations of the source-lens-observer system without any small-angle limitations. This is done for any spherically symmetric black holes and for the equatorial plane of Kerr black holes. In light of this formalism we revisit the previous literature on retrolensing, sensibly improving the observational estimates. In particular, for the case of the star S2, we give precise predictions for the magnitude of the relativistic images and the time of their highest brightness, which should occur at the beginning of A.D. 2018. The observation of such images would open fascinating perspectives on the measure of the physical parameters of the central black hole, including mass, spin, and distance.

Subject headings: black hole physics — Galaxy: center — gravitational lensing — stars: individual (S2)

1. INTRODUCTION

The fact that light rays can wind an arbitrary number of times around a black hole before emerging back toward spatial infinity has been well known since the earliest studies of general relativity (Darwin 1959; Atkinson 1965; Luminet 1979; Ohanian 1987; Nemiroff 1993; see also the treatment in Chandrasekhar 1983). In practice, a source behind a black hole produces not only the two classical weak-field gravitational lensing images but also an infinite number of strong-field images corresponding to photons with winding numbers running from 1 to infinity. This phenomenon has been revived in a work by Virbhadra & Ellis (2000), who showed that the supermassive black hole at the center of our Galaxy may be a suitable lens candidate. The resolution needed for such an observation is very high but should be reached by future very long baseline interferometry experiments such as ARISE⁵ and MAXIM.⁶ In order to describe gravitational lensing in such extreme cases, we cannot use any weak-field approximation. However, it is possible to take advantage of the opposite limit and finally get a very simple and efficient analytical approximation, called the strong-field limit (SFL; Bozza 2002). This method first emerged in Schwarzschild black hole studies (Darwin 1959; Ohanian 1987; Bozza et al. 2001), then was applied to Reissner-Nordstrom black holes (Eiroa et al. 2002) and to charged black holes of heterotic string theory (Bhadra 2003) and finally generalized to an arbitrary spherically symmetric metric (Bozza 2002). The microlensing situation was

considered by Petters (2003), while Kerr black holes were explored analytically for quasi-equatorial motion (Bozza 2003) and numerically for arbitrary motion (Vazquez & Esteban 2003). It is also interesting that a time-delay measurement would give a precise estimate of the distance of the lens (Bozza & Mancini 2004). For former and/or alternative formulations of strong-field gravitational lensing see Frittelli & Newman (1999), Frittelli et al. (2000), Dabrowski & Schunck (2000), and Perlick (2004).

Already in the first studies of gravitational lensing in strong fields by Darwin (1959) it was noticed that the whole sky is mapped in the vicinity of what was then called a “compact sun.” In particular, it was known that a source in front of the lens could yield relativistic images and Einstein rings as bright as a source behind the lens (see, e.g., Luminet 1979). In more recent years retrolensing was rediscovered quite independently from standard gravitational lensing. Holz & Wheeler (2002) proposed that a black hole of a few solar masses passing within 1 pc of the solar system would redirect photons from the Sun backward to the Earth. An observer would thus see a “star” lighting up and then switching off in the sky as the Earth in its motion enters and leaves the best alignment position. De Paolis et al. (2003) suggested the black hole in Sgr A* at the center of our Galaxy as a suitable retrolens, proposing the star S2 (the star with the smallest average distance from Sgr A* discovered so far) as a candidate source. At the moment, this seems to be the best known candidate for gravitational lensing in strong fields, deserving a closer investigation. At the same time, Eiroa & Torres (2004) considered retrolensing by Sgr A*, using the analytical framework of the SFL method to give correct estimates for such a phenomenon; their investigation, however, is limited to small angles and cannot cover the case of S2. Finally, De Paolis et al. (2004) extended Holz & Wheeler’s proposal to Kerr retrolensing, using the SFL method to calculate the position of the images but using the Holz & Wheeler formula for the amplification (which is inadequate for spinning black holes), finding no significant deviation from the light curves of the Schwarzschild case.

¹ Centro Studi e Ricerche “Enrico Fermi,” via Panisperna 89/A, Rome, Italy.

² Dipartimento di Fisica “E.R. Caianiello,” Università di Salerno, via S. Allende, Baronissi (SA) I-84081, Italy.

³ Istituto Nazionale di Fisica Nucleare, Sezione di Napoli, Complesso Universitario di Monte Sant’Angelo, Via Cintia, 80126 Naples, Italy.

⁴ Institut für Theoretische Physik der Universität Zürich, CH-8057 Zürich, Switzerland.

⁵ For more about ARISE see: <http://spacelink.nasa.gov/nasa.projects/space.science/universe/arise.Mission/>.

⁶ The MAXIM Web site is at <http://maxim.gsfc.nasa.gov>.

In this paper, we give up any limitation due to small-angle approximation and treat the standard and retro-gravitational lensing on a unified ground, where they just come up as particular cases. In addition to recovering these two situations, we also address the gravitational lensing problem for any intermediate geometries, in which the strong-field images are still present as always but are usually dimmer (see § 2). This allows us to treat in a very accurate way the case of the star S2, giving precise predictions for the light curves of its images in the next several years. Moreover, we clarify several aspects that were not clearly stated in the former literature, constructing a unique analytical framework for the whole phenomenology.

In § 2 we discuss the spherically symmetric lens; we give the formulae for the position and the magnification of the images and discuss the differences with the magnification formula by Holz & Wheeler (2002); we also comment on the importance of time-delay measurements. Section 3 is devoted to the study of S2, the best candidate source for gravitational lensing in the SFL; we use our formalism to draw analytical curves of the images, accurately predicting the epoch of their luminosity peak. In § 4, in the light of the results by Bozza (2003), we guess about the possible changes in S2 relativistic images if the black hole at the center of our galaxy has nonvanishing spin; we also compare our results in Sun retrolensing by Kerr black holes with those by De Paolis et al. (2004). Section 5 contains a summary of the work.

2. GRAVITATIONAL LENSING BY SPHERICALLY SYMMETRIC BLACK HOLES

According to the SFL method, the deflection angle of a light ray passing very close to a black hole can be expanded around the minimum impact angle θ_m , which separates the light rays absorbed by the black hole ($\theta < \theta_m$) from the light rays that are simply deflected ($\theta > \theta_m$). As previously shown (Bozza 2002), the deflection angle always diverges logarithmically at $\theta \sim \theta_m$ for any class of spherically symmetric black holes. The logarithmic term and the constant term give a sufficient approximation to the deflection angle in order to explain the whole phenomenology. The fundamental formula reads

$$\alpha(\theta) = -\bar{a} \log\left(\frac{\theta}{\theta_m} - 1\right) + \bar{b}, \quad (1)$$

up to higher-order terms in $(\theta - \theta_m)$. The numerical coefficients \bar{a} and \bar{b} depend on the characteristics of the black hole (electric charge, coupling to a scalar field, the particular gravitational theory we are using, etc.). We refer the reader to (Bozza 2002) for its full derivation and for some examples (see also Bhadra 2003).

Using equation (1), Eiroa & Torres (2004) have correctly calculated the position and the magnification of the retrolensing images. However, their treatment (as well as the treatment in Bozza 2002 for standard lensing) is limited to small separations of the source from the optical axis (defined as the line connecting the observer with the lens). In order to address the general case, we have to write the lens equation in a suitable way, without restricting to particular cases.

2.1. Lens Equation and Position of the Images

The source, the lens, and the observer define the plane where the whole motion of the photon takes place in the case of spherically symmetric black holes. We define γ as the angle between the source-lens direction and the optical axis (see

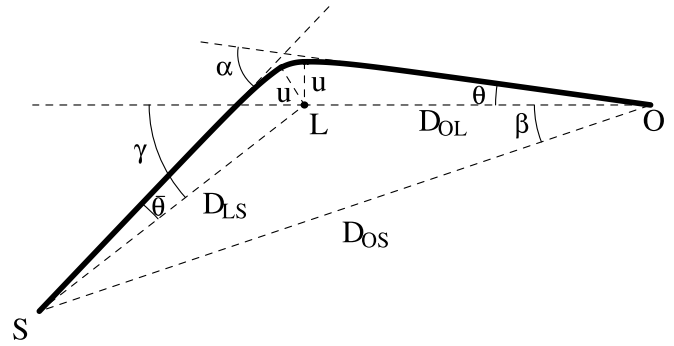


FIG. 1.—Generic lensing configuration.

Fig. 1), and θ as the angular position of the image in the sky of the observer with respect to the position of the black hole, which coincides with the impact angle of the light ray as seen by the observer. The impact angle as seen from the source is called $\bar{\theta}$. Then the lens equation is simply (see also Bozza 2003)

$$\gamma = \alpha(\theta) - \theta - \bar{\theta}. \quad (2)$$

Now, we can give a unique treatment allowing γ to run over the whole range $[0, +\infty)$. In fact, $\gamma \simeq 0$ would yield the weak-field gravitational lensing, $\gamma \simeq \pi$ would be gravitational retrolensing, $\gamma \simeq 2\pi$ would give standard gravitational lensing in the SFL, and so on. The collection of strong-field gravitational lensing images would be recovered, solving the lens equation for $\gamma \simeq 2n\pi$ with $n \geq 1$, while the collection of retrolensing images is recovered with $\gamma = (2n - 1)\pi$ with $n \geq 1$.

Since we are only interested in strong-field gravitational lensing of far sources, the impact angle $\theta = \arcsin(u/D_{OL})$ is always negligible compared to γ and α , as it is of the order of the Schwarzschild radius of the black hole divided by the distance of the lens, which is usually much larger (unless we are falling into the black hole). So we can safely drop θ from equation (2). For $\bar{\theta}$ we can apply the same argument as long as the source is far enough from the black hole (see, e.g., Cunningham & Bardeen 1973 or Viergutz 1993 for the more complicated case where the source is orbiting very close to the black hole).

The general solution of the lens equation is then

$$\theta = \theta_m \left[1 + e^{(\bar{b}-\gamma)/\bar{a}} \right]. \quad (3)$$

This formula is valid both for standard gravitational lensing (when $\gamma \simeq 2n\pi$; compare with Bozza 2002) and for retrolensing [when $\gamma \simeq (2n - 1)\pi$; compare with Eiroa & Torres 2004]. It is also valid for any intermediate situation. Its limits of validity are fixed by the accuracy of the SFL formula (eq. [1]) for the deflection angle when we slip from strong-field to weak-field gravitational lensing. This point deserves a deeper discussion.

Estimates of the accuracy of the SFL approximation are easily made in the Schwarzschild case, where it is possible to calculate the deflection angle exactly (Bozza et al. 2001). So let us call $\alpha_{\text{ex}}(\theta)$ the exact deflection angle for Schwarzschild black hole. Let θ_{ex} be the image calculated using α_{ex} in the lens equation (2). What is really interesting in the images is the difference from the minimum impact angle, i.e., $\theta - \theta_m$ and $\theta_{\text{ex}} - \theta_m$. So, in Figure 2 we finally plot $(\theta_{\text{ex}} - \theta_m)/(\theta_{\text{ex}} - \theta_m)$ versus γ .

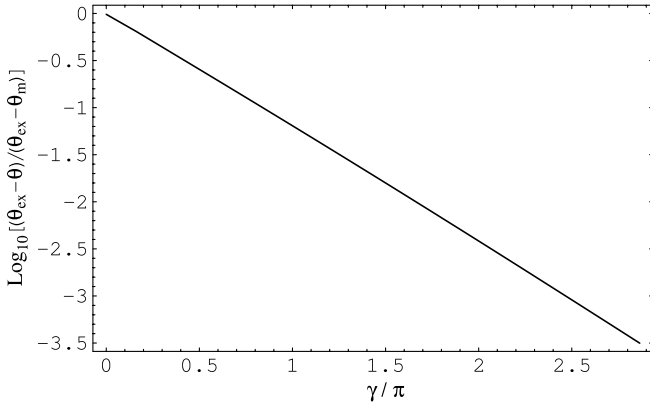


FIG. 2.—Accuracy of the SFL in the determination of the images as a function of the source position angle γ .

Of course when $\gamma \simeq 0$, we should rather use the weak-field approximation, and the error becomes very large. (We should also take into account the fact that the additional terms in the lens equation are no longer negligible.) What is more interesting is looking at the error in the determination of the retrolensing images ($\gamma \simeq \pi$), which turns to be of the order of 6%. The accuracy grows exponentially with γ , so that the outermost relativistic image of standard strong-field gravitational lensing ($\gamma = 2\pi$) is determined with an accuracy of 0.3%. To improve these numbers, which is perhaps desirable for the outermost retrolensing image, higher-order terms in the formula for the deflection angle should be included, but this task is beyond the scope of this work. A 6% accuracy in retrolensing will be sufficient for most of the following discussions.

2.2. Magnification of the Images

In the first retrolensing paper, Holz & Wheeler (2002) proposed a rather unusual formula for the amplification of the images, based on heuristic arguments:

$$A = \pi(u_o^2 - u_i^2) \frac{\Delta\Theta}{2\pi}, \quad (4)$$

$$\Delta\Theta = 2 \arctan\left(\frac{R_S}{D_{OS} \sin \beta}\right), \quad (5)$$

where u_i and u_o are the inner and outer impact parameters that bound the image, respectively, $\Delta\Theta$ is the amplitude of the arc described by the image, and R_S is the source radius.

According to this formula, a full Einstein ring would form only for a perfect alignment $\beta = 0$. This is obviously wrong, since it is sufficient that just one point of the source is perfectly aligned to build a full Einstein ring. For a source far enough from perfect alignment, it can be shown that this approximate formula coincides with the standard formula we derive in this subsection. However, it cannot be trusted in the high-alignment regime and should be replaced by a more rigorous one.

Ohanian (1987) already derived a formula valid for the Schwarzschild black hole. Here we rederive it for an arbitrary black hole. To describe the extension of the source in terms of our angles, we can attach polar coordinates to the lens frame, where γ plays the role of the polar angle from the optical axis, and we introduce an azimuthal angle ϕ around this axis. Then the solid-angle element is given by $d\omega_S = d\gamma \sin \gamma d\phi$. In the

same way, we can attach polar coordinates to the observer obtaining an image element $d\omega_I = d\theta \sin \theta d\phi$. The quantity

$$\frac{d\omega_I}{d\omega_S} = \frac{\sin \theta}{\sin \gamma (d\gamma/d\theta)} \quad (6)$$

represents the ratio between the angular extension of the image as it appears to the observer and the extension of the source as it appears to the black hole. The latter is related to the extension of the source as it appears to the observer by the simple quadratic ratio of the distances D_{OS}^2/D_{LS}^2 . Finally we have

$$\mu = \frac{D_{OS}^2}{D_{LS}^2} \frac{\sin \theta}{\sin \gamma (d\gamma/d\theta)}. \quad (7)$$

The source distance is, of course, related to the other distances by simple trigonometry: $D_{OS}^2 = D_{OL}^2 + D_{LS}^2 + 2D_{OL}D_{LS} \cos \gamma$. Moreover, since we are always considering black holes far from the observer, we can safely approximate $\sin \theta \simeq \theta$. On the other hand, only for a high-alignment situation, with $\gamma \simeq k\pi$, can we replace $\sin \gamma$ by $|\gamma - k\pi|$. In such cases, which correspond to standard and retrolensing, we recover the usual formula for the magnification of spherically symmetric lenses, valid for small angles. Equation (7), on the contrary, is valid also for a general γ .

Now, using the lens equation, we can write

$$\mu = -\frac{D_{OS}^2}{D_{LS}^2} \frac{\theta_m^2 e^{(\bar{b}-\gamma)/\bar{a}} [1 + e^{(\bar{b}-\gamma)/\bar{a}}]}{\bar{a} \sin \gamma}, \quad (8)$$

where the sign coming out of the derivative correctly accounts for the parity of the image. For $\gamma \simeq 2n\pi$ we recover the magnification formula given by Bozza (2002), while for $\gamma \simeq (2n-1)\pi$ we recover the formula given by Eiroa & Torres (2004). However, equation (8) smoothly joins the two extreme cases, covering the whole range of γ . It can be obtained from the Kerr magnification formula given by Bozza (2003) in the limit of vanishing black hole spin. In addition, the derivation proposed here does not need to pass through the Kerr metric and can be applied to a generic spherically symmetric black hole.

The caustic points (points of formally infinite magnification) are exactly at $\gamma = k\pi$ where $\sin \gamma$ vanishes. Sources close to these points get the maximal amplification. That is why standard and retrolensing were first studied as the most interesting physical cases.

To treat extended sources we need to integrate this formula over the angular extension of the source, eventually weighted by a surface brightness factor. If the source is far from a caustic point, then the magnification varies very little along the source surface, and it makes almost no difference to approximate the source as a point. On the other hand, the magnification for pointlike sources diverges on caustic points, while for realistic extended sources we get a finite result integrating over the source angular area. Then the source radius acts as an effective cutoff of the magnification.

In order to compare this formula with that of Holz & Wheeler (2002), we can use it in the limit of retrolensing, with $\gamma \simeq \pi$. The magnification becomes

$$\mu_{\text{retro}} = -\frac{D_{OS}^2}{D_{LS}^2} \frac{\theta_m^2 e^{(\bar{b}-\pi)/\bar{a}} [1 + e^{(\bar{b}-\pi)/\bar{a}}]}{\bar{a} |\gamma - \pi|}, \quad (9)$$

where we have neglected the dependence on γ in the exponentials being much weaker than the dependence in the denominator.

Finally, the integral over the source extension for a constant brightness source of radius R_S is a standard calculation in terms of elliptic functions, first performed by Witt & Mao (1994) and also given explicitly by Eiroa & Torres (2004). It amounts to replacing the $|\gamma - \pi|^{-1}$ in equation (9) by its integral over the source disk D_S ,

$$\begin{aligned} \frac{1}{\pi\gamma_S^2} \int_{D_S} \frac{1}{\gamma} \sin \gamma d\gamma d\phi = \\ \frac{2\text{sign}[\gamma_S - \gamma]}{\pi\gamma_S^2} \left[(\gamma_S - \gamma)E\left(\frac{\pi}{2}, -\frac{4\gamma_S\gamma}{(\gamma_S - \gamma)^2}\right) \right. \\ \left. + (\gamma_S + \gamma)F\left(\frac{\pi}{2}, -\frac{4\gamma_S\gamma}{(\gamma_S - \gamma)^2}\right) \right], \quad (10) \end{aligned}$$

where for simplicity we have used γ instead of $|\gamma - \pi|$ and we have defined $\gamma_S = R_S/D_{LS}$; F and E are the elliptic integrals of first and second kind.

With this formula, we can draw a retro-MACHO light curve for the situation described by Holz & Wheeler (2002), i.e., a black hole of $10 M_\odot$ passing at 0.01 pc from the Sun, which deviates photons coming from the Sun backward to the Earth. We can compare the curves in Figure 3 with those by Holz & Wheeler (2002) to see how different the shape looks when the source starts to cover the caustic point (*top curve*). It is interesting to note that the absolute normalization of the curves by Holz & Wheeler (2002) is slightly different from that by De Paolis et al. (2004), and both are slightly different from ours. This might depend on minor approximations in the units of measure.

In the case of perfect alignment, equation (10) gives $2/\gamma_S$. The maximum amplification is thus

$$\mu_{\max} = \frac{D_{OS}^2}{D_{LS}^2} \frac{4\theta_m^2 e^{(\bar{b}-k\pi)/\bar{a}} [1 + e^{(\bar{b}-k\pi)/\bar{a}}]}{\bar{a}\gamma_S}, \quad (11)$$

where we have also multiplied by two in order to sum the (equal) magnifications of the two images. In Sun retrolensing, it amounts to

$$\mu_{\max} = 1.29 \times 10^{-14} \left(\frac{M_L}{10 M_\odot}\right)^2 \left(\frac{R_S}{R_\odot}\right)^{-1} \left(\frac{D_{OL}}{0.01 \text{ pc}}\right)^{-1}. \quad (12)$$

Now, let us consider an arbitrary geometry, where observer, source, and lens are completely misaligned, so that γ is far from $k\pi$. Then we have to use the general equation (7) for the magnification with a value for $\sin \gamma$, which is a generic number between 0 and 1. To compare this situation with the perfect alignment, we can take the ratio between equation (7) with $\sin \gamma \simeq 1$ and one-half of equation (11) (for a single image). Apart from the exponentials, which can weakly modify the order of magnitude, this ratio is generally of the order of

$$\frac{\mu_{\min}}{\mu_{\max}} \sim \frac{\gamma_S}{2} \ll 1. \quad (13)$$

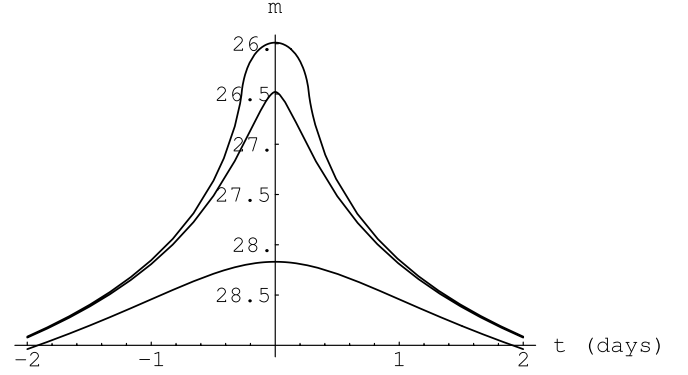


FIG. 3.—Total magnitude of the images of the Sun produced by a black hole with $10 M_\odot$ at 0.01 pc distance acting as a retrolens. From bottom to top we consider a central event, an event with maximum alignment of $\gamma = 1 R_\odot/D_{LS}$, and one with $\gamma = 1 \text{ AU}/D_{LS}$.

Thus, intermediate lensing is generally disfavored with respect to standard and retro-gravitational lensing. However, this does not mean that intermediate lensing cannot be interesting from an observational point of view, as we shall see in § 3.

2.3. Time Delay in Strong-Field Gravitational Lensing

Time delay in strong-field gravitational lensing provides a very important independent observable, which directly yields the distance of the lens with a good accuracy (Bozza & Mancini 2004). In fact, the time delay between images with successive winding numbers is

$$\Delta T = 2\pi \frac{D_{OL}\theta_m}{c_0}, \quad (14)$$

where c_0 is the speed of light. Thus, by measuring θ_m and ΔT we can immediately obtain D_{OL} . To get an idea of how big the time delay is, we can write it as

$$\Delta T = 0.13h \left(\frac{M}{2.87 \times 10^6 M_\odot}\right). \quad (15)$$

It is thus completely insignificant for solar mass black holes, even if they are close to our solar system. It is also quite small for the black hole at the center of our Galaxy, but it amounts to several days for supermassive black holes in other galaxies, being thus measurable, once we find a suitable variable source.

The calculations by Bozza & Mancini (2004) were made with the standard gravitational lensing configuration in mind. However, it is easy to see that in retrolensing or any intermediate lensing configurations the time difference between relativistic images remains exactly the same, while only the (unobservable) absolute travel time of the photon changes.

Now let us consider the time delay between the first relativistic image and the direct image of the source. When the source is well aligned behind the lens, then the direct image becomes weakly lensed and the first relativistic image turns to the secondary weak-field image. In this case, the Shapiro time-delay formula applies (see Wex et al. 1996 for an application involving the Galactic center).

If the source is not behind the lens, then the time delay between the first relativistic image and the direct image is dominated by the geometric path difference

$$\begin{aligned} \Delta T &= \frac{D_{OL} + D_{LS} - D_{OS}}{c_0} = \frac{D_{OL}}{c_0} \left[1 + \frac{\sin \beta - \sin \gamma}{\sin(\gamma - \beta)} \right] \\ &\simeq \frac{D_{OL}}{c_0} \frac{1 - \cos \gamma}{\sin \gamma} \beta, \end{aligned} \quad (16)$$

where β is the angular separation between the source and the black hole as seen by the observer. The last approximate equality is valid if $\beta \ll 1$. In principle, by measuring β and ΔT , if we have a good knowledge of γ , we can use the time delay to estimate the distance to the lens. With respect to the time delay between consecutive relativistic images, this measure is surely easier, since we just need one relativistic image. However, we need a good knowledge of the angle γ , which was not required in the previous case.

3. GRAVITATIONAL LENSING OF THE STAR S2 BY SGR A*

S2 is the star with the least average distance from the Galactic center discovered so far (Schödel et al. 2002). Its orbital motion has been very accurately reconstructed through proper motion and spectral measurements. Its orbital parameters, taken by Schödel et al. (2003), are reported in Table 1. This star looks like an O8–B0 main-sequence star of $15 M_\odot$ with an apparent magnitude in the K band (centered on $\lambda = 2.2 \mu\text{m}$) of $m_K = 13.9$. The extinction in the K band in the region of the Galactic center amounts to 3.3 mag (Rieke et al. 1989). The orbital period and the semimajor axis fix the enclosed mass to $M_{\text{enc}} = 3.3 \times 10^6 M_\odot$, slightly larger than the central black hole mass, which is currently estimated as $M_{\text{BH}} = 2.87 \times 10^6 M_\odot$.

The value of the inclination of the orbit suggests that a high alignment with the observer-lens line does not occur during the motion of the star around Sgr A*. This seems to rule out any possibility for standard or retro-gravitational lensing. Contrarily to what was expected, De Paolis et al. (2003) claimed that the relativistic images of S2 near the central black hole are not far beyond instrumental sensitivities, even if the alignment is not favorable. In this section we complete their analysis in the light of our formalism, including all the significant orbital parameters and drawing light curves for the relativistic images using our magnification formula. We can thus confirm their claim, also predicting the best observability time for these images.

TABLE 1
ORBITAL PARAMETERS FOR S2

Orbital Parameter ^a	Value
a	4.54×10^{-3} pc
P	15.73 yr
e	0.87
T_0	2002.31 yr
i	$45^\circ 7$
Ω	$45^\circ 9$
ω	$244^\circ 7$

^a Parameters: a is the semimajor axis, P is the orbital period, e is the eccentricity, T_0 is the epoch of periape, i is the inclination of the normal of the orbit with respect to the line of sight, Ω is the position angle of the ascending node, ω is the periape anomaly with respect to the ascending node. Data taken from Schödel et al. (2003).

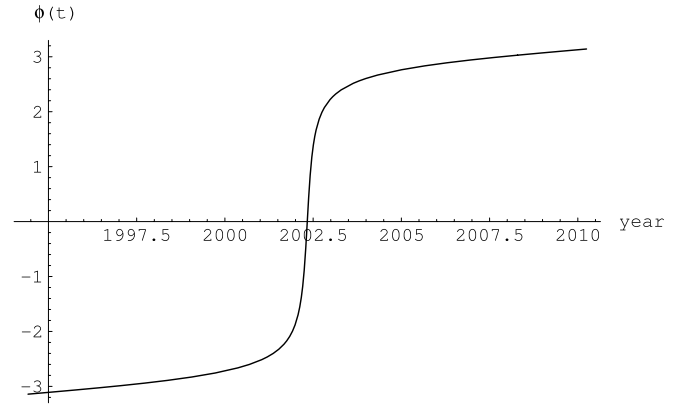


FIG. 4.—Orbital position of S2 as a function of time.

Rather than a retrolensing configuration, S2 represents a case with an intermediate γ . The magnification of the images is thus well described by equation (7). Since the radius of S2 is a few solar radii, γ_S stays much smaller than $|\gamma - k\pi|$ (i.e., we are far enough from caustic points), allowing us to trust the pointlike magnification without the need to integrate it over the source surface. After some algebra, we can write down all the interesting quantities in terms of the orbital parameters of the system:

$$D_{LS} = \frac{a(1 - e^2)}{1 + e \cos \phi}, \quad (17)$$

$$D_{OL} \simeq D_{OS} = 8 \text{ kpc}, \quad (18)$$

$$\gamma = \arccos[\sin(\phi + \omega) \sin i], \quad (19)$$

where ϕ is the anomaly angle of the star starting from the periape epoch, i is the inclination of the orbit, and ω is the periape anomaly with respect to the ascending node. By the angular momentum conservation, we have

$$L = M_{S2} \sqrt{GM_{\text{enc}} a (1 - e^2)} = M_{S2} D_{LS}^2 \dot{\phi}. \quad (20)$$

By this equation, we can write a differential equation for $\dot{\phi}$,

$$\frac{[a(1 - e^2)]^{3/2}}{\sqrt{GM_{\text{enc}}(1 + e \cos \phi)^2}} \dot{\phi} = 1. \quad (21)$$

Integrating and inverting, we can get ϕ as a function of time, exploiting the initial condition $\phi(T_0) = 0$, with T_0 given in Table 1. If the eccentricity of the orbit of S2 were negligible, $\phi(t)$ would just be a linear function of time, of the form $\phi(t) = \omega_0 t$, with $\omega_0 = 2\pi/T$ being a constant. This approximation was done for simplicity by De Paolis et al. (2003). However, in Figure 4 we see that the high value of the eccentricity drastically modifies this function. To get accurate predictions, it is thus mandatory to take into account the angular motion of S2 correctly.

Finally, we can plot the magnification of the first two relativistic images, taking $M_{\text{BH}} = 2.87 \times 10^6 M_\odot$ as the mass of the black hole (Schödel et al. 2003; De Paolis et al. 2003 used M_{enc}). The first relativistic image has $0 < \gamma < \pi$. In practice it is the secondary image of weak-field gravitational lensing that turns into a strong-field image because of the high misalignment. It has a negative parity and is formed close to the black hole on the other side with respect to the direction of S2. The

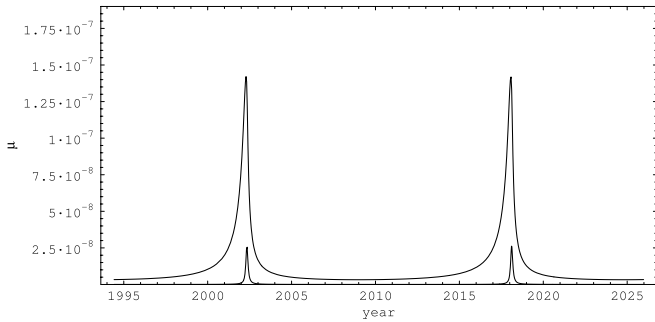


FIG. 5.—Magnification of the first two relativistic images as a function of time.

second relativistic image has $\pi < \gamma < 2\pi$ and comes from light rays which take the “wrong” direction around the black hole and are bound to turn once more around it in order to reach the observer. This image has positive parity and appears on the same side of S2. The next images are fainter and probably uninteresting for the moment.

In Figure 5 we plot the magnifications of the first two images as functions of time. The periaapse epoch is the most favorable for the observations, since D_{LS} , which appears with a power of -2 in equation (7), drops to its minimum value. This minimum value is still 1300 times larger than the Schwarzschild radius of the central black hole, so that we can safely treat the source as far from the lens. Since the angular velocity of S2 is maximal in the periaapse epoch, the luminosity peak is relatively short. As S2 passed through the periaapse in 2002, we have to wait for the next periaapse to get this luminosity peak. In Figure 6 we have drawn the expected apparent magnitudes in the K band of the first two relativistic images at the epoch of the next periaapse, supposing that the extinction value 3.3 in this band (Rieke et al. 1989) also applies from light coming to us from regions very close to the central black hole. The first relativistic image should stay brighter than 32 mag from mid-August 2017 to mid-April 2018. The second relativistic image is typically 5.4 times fainter during the peak, a hard challenge for next-generation instruments.

The observation of a relativistic image requires a strikingly high angular resolution together with a high flux sensitivity. Very impressive improvements in very long baseline interferometry have been performed in recent years in the radio bands. With the first detection of transatlantic fringes at 147 GHz (Krichbaum et al. 2002), the present world record has been established at $18 \mu\text{as}$, which is just a few times the angular size of the Schwarzschild radius of the black hole at the Galactic center. Further improvements can be obtained at submillimeter wavelengths.

A very important step for absolute sensitivity in the infrared band is the *James Webb Space Telescope (JWST)*, which will operate in the wavelength interval $0.6\text{--}27 \mu\text{m}$. At $\lambda = 2.2 \mu\text{m}$ with a 3 hr exposure, it will be able to detect a flux corresponding to 32 mag, just enough to catch the first S2 relativistic image. If coupled with other instruments still to come, then the detection of relativistic images could become a future observational frontier. Furthermore, we cannot forget that the Galactic center is surrounded by a crowded cluster of stars, which can probably yield even better candidates than S2 for strong-field gravitational lensing.

We close this section with some comments on possible time-delay measurements. Since S2 is close to the center of the Galaxy but never aligned behind it, we can estimate the

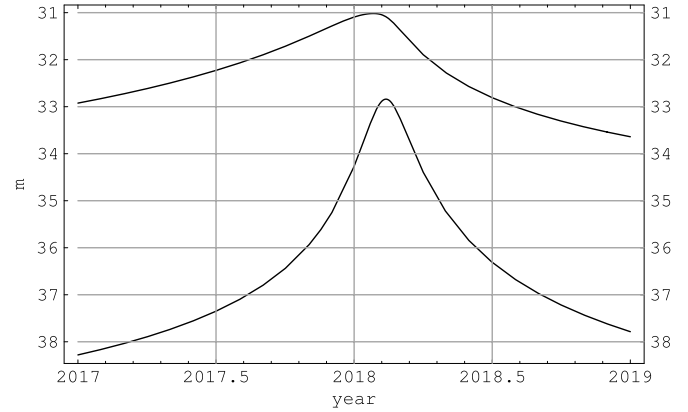


FIG. 6.—Apparent magnitude of the first two relativistic images in the epoch of the next periaapse.

time delay between the first relativistic image and the direct image using equation (16). At the luminosity peak epoch, this delay amounts to 5.95 hr, thus being comparable to the exposure time. In the particular case of S2, no intrinsic variability has been reported up to now in the observed spectral bands. However, the principle of time-delay measures could be applied to eventual new candidates or to S2 itself if any variability is detected in its flux. A measure of such a short time delay requires a very good sampling over the whole period of variability. The precision of such an estimate is limited by the effort undertaken to sample the two light curves to be compared. With a good knowledge of the orbit (in order to correctly estimate γ) and a sufficient sampling, which would depend on the future facilities and the characteristics of the source, it could be possible to establish the distance to the center of the Galaxy on a solid direct measurement.

4. KERR GRAVITATIONAL LENSING

What we have said up to now is true for spherically symmetric black holes (including the estimates on S2 gravitational lensing). In the case of spinning black holes, everything becomes much more complicated, but some very important facts already emerge from the analysis of quasi-equatorial motion, which has already been done analytically (Bozza 2003). In fact, it is evident that the caustics are no longer aligned along the optical axis, but drift following the sense of rotation of the black hole. In addition, they are no longer pointlike but acquire finite extension. To get an idea of the importance of these changes, we can see that for $a = 0.1$, the first retrolensing caustic drifts from the optical axis by an angle of 10° and acquires an extension of 2.4 on the equatorial plane. The existence of extended caustics is accompanied by the formation of pairs of additional images when the source enters one of the caustics. These images are missed in the quasi-equatorial approach, since they rather live far from the equatorial plane. A very important consequence is the fact that high magnifications can be attained much more easily. In fact, while in spherically symmetric metrics the caustics are pointlike and coincide with the optical axis, in the Kerr metric they are distributed in all directions around the lens and have finite extension, so that it is much easier for a source to lie within a high-amplification region for some relativistic images. Another complication arises because the usual hierarchy among relativistic images, which just follows the winding number, can be completely upset by the fact that the

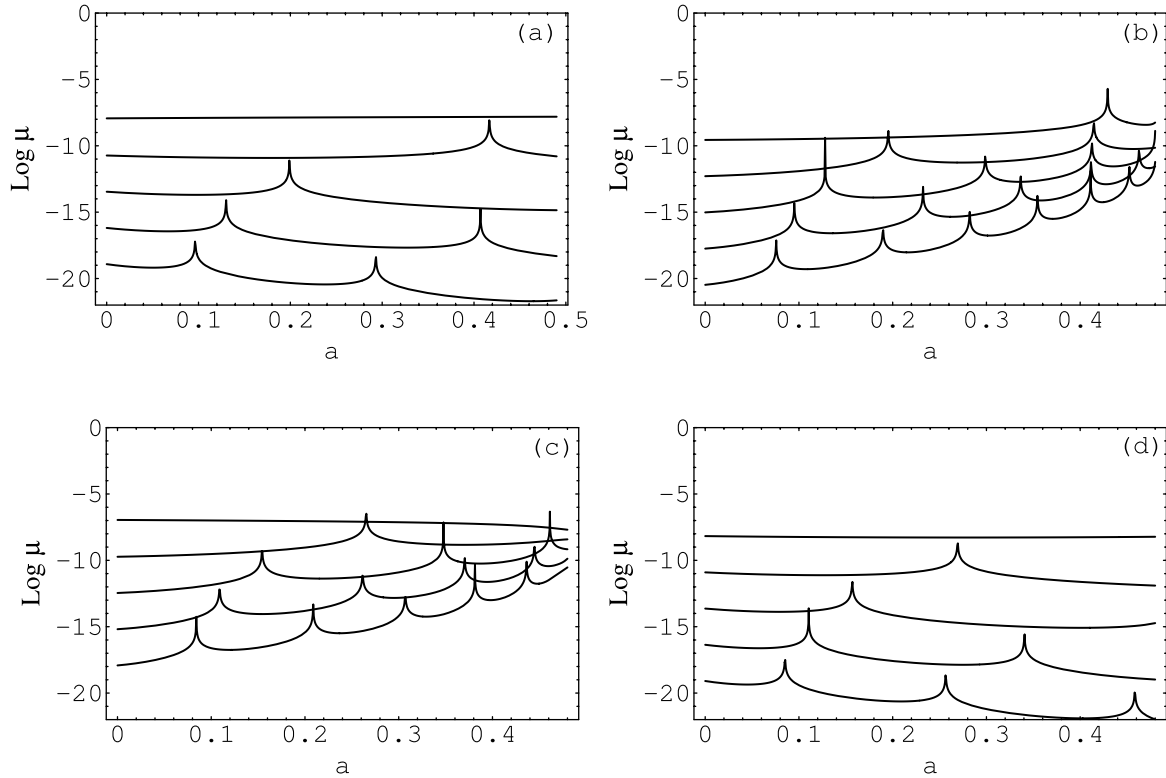


FIG. 7.—Magnifications of the images of S2 as functions of the black hole spin a at (a, b) time $t_1 = 2003.12$; and (c, d) time $t_2 = 2018.00$. Panels (a) and (c) are the negative parity images with increasing winding numbers, and (b) and (d) are the positive parity images, again with increasing winding numbers.

source lies in a caustic that affects images with a higher winding number.

Summing up, Kerr black hole lensing is much richer than spherically symmetric black hole lensing. It is also much more promising from a phenomenological point of view, since it is easier to have brighter images. And of course, it is reasonable to expect that astrophysical black holes are born with a non-negligible spin. All these statements point to the importance of the investigation of Kerr black hole lensing in the general case.

4.1. Kerr Black Hole Lensing with S2

As a practical example of the modifications that an eventual spin of the black hole in Sgr A* would have on the light curve of the images of S2, let us calculate the magnification at the moments when S2 crosses the plane of the Galaxy. It is reasonable to assume that if the central black hole is spinning, the angle of its equatorial plane is very close to that of the rotational plane of the Galaxy. Using the orbital parameters of S2, we see that it has crossed the Galactic plane in $t_1 = 2003.12$, where it had $\gamma = 77.2$ and $D_{LS} = 2.74 \times 10^{-3}$ pc, being east of the black hole and slightly behind it. It will cross the Galactic plane again in $t_2 = 2018.00$ with $\gamma = 102.5$ and $D_{LS} = 6.93 \times 10^{-4}$ pc, being west of the black hole and slightly before it. For these crossing times, we can precisely calculate the magnifications of the equatorial images using the formula by Bozza (2003),

$$\mu = \frac{D_{OS}^2}{D_{OL}D_{LS}} \times \frac{\sqrt{u^2 - a^2}u}{\bar{a} \left| \sqrt{u^2 - a^2}(D_{OL} + D_{LS})C - D_{OL}D_{LS}S \right|}, \quad (22)$$

where $u = \theta R_{\text{Sch}}/D_{OL}$, $C = \cos \bar{\phi}$, $S = \sin \bar{\phi}$, and $\bar{\phi}$ is the phase of the photon oscillations on the equatorial plane, expressed by

$$\bar{\phi} = -\frac{\bar{b} - \gamma}{\bar{a}} + \hat{b}. \quad (23)$$

The coefficients \bar{a} , \bar{b} , and \hat{b} are all functions of the spin of the black hole a , (see Bozza 2003 for the whole derivation).

In Figure 7 we plot the magnifications of the images as a function of the black hole spin, from $a = 0$ (Schwarzschild) to $a = 0.5$ (an extreme Kerr black hole in our normalization). In Figures 7a and 7b we plot the image magnifications for the past time t_1 , while in Figures 7c and 7d we plot the image magnifications for the future time t_2 . In Figures 7a and 7c we plot the magnifications of the images with negative parity. The brightest of them gives the most significant contribution (it is this image that is going to be most likely observable). The magnifications of the images with increasing winding numbers plotted together. The higher the winding number, the lower the magnification. In Figures 7b and 7d we represent the magnification of the positive parity images. The most relevant of these are also represented in Figures 5 and 6, where they are, however, fainter than the brightest negative parity image. As the winding number increases, the magnification decreases. The images in Figures 7a and 7d are formed by retrograde photons, i.e., winding oppositely to the sense of rotation of the black hole. The images in Figures 7b and 7c are formed by corotating photons.

Now let us comment on the outcome of these figures. Increasing the spin of the black hole, we see that corotating images become brighter and retrograde images become fainter. The most striking features are the peaks in the magnification that occur at definite values of the black hole spin. Varying the black hole spin, the caustic points drift all around the

trigonometric interval, and for some values they meet the angular position of S2. Around these values, the magnification can become significantly higher than the normal value. We also see that the first caustics, corresponding to low winding numbers, move slowly and thus cross the position of S2 fewer times. The caustics corresponding to higher winding numbers move quickly. For this reason the fainter images meet caustics more often in the interval of variability of a .

If the true value of the spin of the central black hole is such that one of the images is close to a caustic point, that image will be highly amplified. By these plots, we see that in A.D. 2018.00 for the particular value $a \sim 0.26$, the second negative parity image will overcome the brighter one.

Besides the luminosity of the relativistic images, the presence of a spin for the black hole also affects their position. In fact, images formed by retrograde photons appear up to 1.5 times farther from the central black hole, while corotating photons appear up to 2.6 times closer to it.

Finally, it must be kept in mind that since the caustics have extended areas, these caustic points are actually just the cusps of these caustics. This means that the images we are plotting in Figure 7 change their parity at every caustic crossing. Global parity conservation is assured by creation or destruction of nonequatorial images of the same parity of the image before the crossing. For these images we do not have an analytical treatment at the moment, and all we can say is that they will appear at each caustic crossing and disappear when the source steps out of a caustic.

When a complete analytical treatment of the Kerr black hole lensing is available, not only will we have a clearer idea of the dynamics of all images, but we will be able to use all the information about position and luminosity of all visible relativistic images to measure the spin of the black hole. We can imagine that such an estimate would be much cleaner and simpler than those relying on poorly understood models of the accretion disk or gas surrounding the central black hole, which are subject to very complicated physical processes and dynamics. However, for the details of such a fascinating measure, we still have to wait for further analytical progress on the general Kerr lensing.

4.2. Sun Retrolensing by a Kerr Black Hole

Another context where Kerr black hole lensing was discussed was retrolensing of the Sun by a nearby Kerr black hole (De Paolis et al. 2004). As a first step, a geometry was considered such that the whole event occurred within the equatorial plane of the black hole. Using the formulae by Bozza (2003), the positions of the images were correctly calculated. However, the magnification was estimated using the formula by Holz & Wheeler (2002), which was derived for a Schwarzschild black hole (being also inaccurate for central events, as shown in § 2). It is well known in different contexts (Gould & Loeb 1992; Bozza 1999) that the modification to the magnification map comes firstly from the change to the Jacobian function, due to the change in the lens model, and only secondly from the displacements of the image positions due to the modifications in the lens equation, which can be neglected in a first extent. As a consequence of this simplification, De Paolis et al. (2004) found no significant deviation from Schwarzschild retrolensing. However, by the study of the equatorial case, we learn that the caustics drift and acquire finite extension, so we expect that things are not so simple.

For the configuration considered in Holz & Wheeler (2002) and De Paolis et al. (2004), we have strong magnification only if the source is close to a caustic. Very small misalignments can

kill the images to very small luminosities (it is sufficient to look at Fig. 3 to be convinced; for quantitative estimates see Holz & Wheeler 2002). So, it is sufficient that the relevant caustic for retrolensing moves out of the Earth orbit in order for the Sun retrolensing to disappear at all. With a black hole at a distance of 0.01 pc, this happens if the black hole spin is $a > 0.00027$, quite a small value. If we have a black hole with a spin less than this, then the retrolensing caustic area would be much smaller than the Sun angular radius as seen from the black hole, being effectively treatable as pointlike. Then everything would work more or less like in the Schwarzschild case, with corrections to the magnification curves of the order of $\delta\mu/\mu \simeq a$, i.e., below the precision of SFL approximation.

5. CONCLUSIONS

Gravitational lensing in strong fields is a very interesting subject from the theoretical point of view. Potentially it is a very appealing phenomenon, which is completely embedded within full general relativity. It would thus be an exceptional probe for physics in the regions close to the event horizons of black holes and would give very important feedback on the correct theory of gravitation. This justifies the very strong efforts that have been made by several groups to find possible candidate sources and lenses that could make this fascinating phenomenon manifest. The astrophysical cases investigated up to now are such that the relativistic images should be “almost” observable or should become observable in not too many years. The most important problem is whether these theoretical configurations are likely or not. The case of S2, on the contrary, is a concrete case in which definite predictions for the image luminosities can be made.

In this work we have extended the analytical framework of the strong-field limit analysis to cover all the possible geometric configurations, giving up any small-angle approximations that are not automatically encoded in the tracks of the light rays. In this way, we have been able to revisit the so-called retrolensing, in particular the Sun retrolensing proposed by Holz & Wheeler (2002), with more valid mathematical instruments. Moreover, we can adequately cover any intermediate case, such as that of the star S2 (De Paolis et al. 2003). For the first relativistic image of this star, we predict an epoch of maximal luminosity (better than 32 mag) between the end of A.D. 2017 and the first part of 2018.

Using previous work on equatorial Kerr lensing (Bozza 2003), we have guessed how the presence of extended caustics and their drift from the optical axis can affect the brightness of the relativistic images of S2 at the epoch of its crossing through the Galactic plane. We have also put upper limits on the black hole spin in Kerr retrolensing of the Sun in order to have still significant images.

As a final remark, we can say that strong-field gravitational lensing opens really fascinating perspectives, like testing general relativity and measuring the distance, the spin, or other physical parameters of the black hole in the Galactic center and in the centers of other galaxies. The nice luminosity estimates for S2 encourage us to look for more stars orbiting very close to the central black hole as new potential candidate sources for such an amazing phenomenon.

We thank the CERN theory department for hospitality. We also thank Gaetano Scarpetta for comments on the manuscript, Francesco De Paolis and Achille Nucita for useful discussions, and our referee for some nice suggestions.

REFERENCES

- Atkinson, R. D. 1965, *AJ*, 70, 517
Bhadra, A. 2003, *Phys. Rev. D*, 67, 103009
Bozza, V. 1999, *A&A*, 348, 311
———. 2002, *Phys. Rev. D*, 66, 103001
———. 2003, *Phys. Rev. D*, 67, 103006
Bozza, V., Capozziello, S., Iovane, G., & Scarpetta, G. 2001, *Gen. Relativ. Gravitation*, 33, 1535
Bozza, V., & Mancini, L. 2004, *Gen. Relativ. Gravitation*, 36, 435
Chandrasekhar, S. 1983, *Mathematical Theory of Black Holes* (Oxford: Clarendon Press)
Cunningham, C. T., & Bardeen, J. M. 1973, *ApJ*, 183, 237
Dabrowski, M. P., & Schunck, F. E. 2000, *ApJ*, 535, 316
Darwin, C. 1959, *Proc. R. Soc. London*, 249, 180
De Paolis, F., Geralico, A., Ingrosso, G., & Nucita, A. A. 2003, *A&A*, 409, 809
De Paolis, F., Geralico, A., Ingrosso, G., Nucita, A. A., & Qadir, A. 2004, *A&A*, 415, 1
Eiroa, E. F., Romero, G. E., & Torres, D. F. 2002, *Phys. Rev. D*, 66, 024010
Eiroa, E. F., & Torres, D. F. 2004, *Phys. Rev. D*, 69, 063004
Frittelli, S., Kling, T. P., & Newman, E. T. 2000, *Phys. Rev. D*, 61, 064021
Frittelli, S., & Newman, E. T. 1999, *Phys. Rev. D*, 59, 124001
Gould, A., & Loeb, A. 1992, *ApJ*, 396, 104
Holz, D. E., & Wheeler, J. A. 2002, *ApJ*, 578, 330
Krichbaum, T. P., et al. 2002, in *Proc. 6th European VLBI Network Symposium*, ed. E. Ros et al. (Bonn: MPI), 125
Luminet, J.-P. 1979, *A&A*, 75, 228
Nemiroff, R. J. 1993, *Am. J. Phys.*, 61, 619
Ohanian, H. C. 1987, *Am. J. Phys.*, 55, 428
Perlick, V. 2004, *Phys. Rev. D*, 69, 064017
Petters, A. O. 2003, *MNRAS*, 338, 457
Rieke, G. H., Rieke, M. J., & Paul, A. E. 1989, *ApJ*, 336, 752
Schödel, R., et al. 2002, *Nature*, 419, 694
———. 2003, *ApJ*, 596, 1015
Vazquez, S. E., & Esteban, E. P. 2003, preprint (gr-qc/0308023)
Viergutz, S. U. 1993, *A&A*, 272, 355
Virbhadra, K. S., & Ellis, G. F. R. 2000, *Phys. Rev. D*, 62, 084003
Wex, N., Gil, J., & Sendyk, M. 1996, *A&A*, 311, 746
Witt, H. J., & Mao, S. 1994, *ApJ*, 430, 505